An Entropy-Based Targetless Real-Time Radar-Lidar Point Cloud Alignment System for Smart Sensor Fusion

Xiaojun Chen
Smart Sensor Fusion Laboratory, SEIEE, Shanghai Jiao Tong University
Shanghai, China
solairechen@sjtu.edu.cn

KC Chang
Dept. of SEOR and C5I Center George Mason University
Fairfax, USA
kchang@gmu.edu

Ting Yuan
Smart Sensor Fusion Laboratory, SEIEE, Shanghai Jiao Tong University
Shanghai, China
tyuan@sjtu.edu.cn

***Abstract*—Autonomous systems pose unique challenges for sensor fusion applications. In multi-sensor scenarios, a real-time data geometric alignment system, from initial online calibration to instant data consistency evaluation, is highly desirable for effective and efficient deployment of autonomy solutions. In this paper, we present an entropy-based real-time geometric alignment system for Radar-Lidar point cloud sensor fusion. The online alignment system is targetless and relies solely on multi-sensor point cloud measurements to form an entroy-based test statistics, requiring no prior information about the perception environment. Specifically, we design a finite mixture model (FMM) as empirical probability density function (PDF) to represent environment as a probabilistic world model. A proper entropy measure of the empirical PDF according to the perception world is then introduced to evaluate the FMM randomness. It can be observed that, even in a generally nonstationary environment, both Radar and Lidar point clouds can still converge to an optimal entropy. The gradual fluctuation of this entropy measure over time can serve as a data consistency metric, enabling the detection of sudden sensor drifts. A scenario study is carried out to evaluate and validate the effectiveness and efficiency of the proposed real-time point-cloud alignment system in real world environments.**

***Index Terms*—Alignment System, Online Calibration, FMM, Entropy**

I. Introduction

Autonomous systems pose unique challenges for sensor fusion applications. Data from different sensors (e.g., Radar and Lidar point clouds) must be geometrically aligned throughout the fusion process, especially in complicated or dynamic environments. Initial geometric calibration can be done off-line but requires a tedious and time-consuming process, leading to serious difficulties in effective and efficient deployment and maintenance. Moreover, even a decent calibration is achieved, factors such as vehicle bumps and aging fixtures can cause the positions of mounted sensors to drift, and thus worsening the sensor fusion performance. A targetless statistical measure with slow fluctuation over time to properly reflect the non-stationary perception environment is then highly desirable for the real-time alignment system, which can handle both initial online calibration and instant data consistency, and thereby improving the system efficiency and robustness.

In the applications of sensor fusion for autonomous systems, commonly used perception sensors are Lidar, Radar and Camera. The geometric alignment can be broadly categorized into target-based and targetless. Target-based approaches relies on auxiliary targets with distinct geometric features, which can serve as reference points for achieving the coordinate transformation among various distributed sensors to a specified center frame. For example, in Lidar-Camera systems, checkerboard is widely used as auxiliary targets for initial calibration[1, 8, 23]; in multi-Lidar systems, various highly reflective materials are commonly used, such as orthogonal planes [5], retro-reflective targets mounted to the poles [7] and reflective conical targets [10]; in multi-radar systems, mainly corner reflectors are used[16]. These methods can achieve high accuracy; however, they also require tedious (off-line) setups, making them impractical for real-time or online geometric alignment in complicated non-stationary environments, and are incapable of evaluating data consistency in real-time.

To overcome these limitations, targetless methods have emerged. Ma et al. [11] performed initial calibration by ensuring the alignment of line features extracted from image and point cloud data. Zhu et al. [24] optimized initial calibration by extracting vehicle from Lidar point clouds and images using a semantic segmentation model. Although these methods avoid tedious offline setups, they still rely on specific natural features present in the environment.

To eliminate the dependence on prior environmental features, a natural approach is to align Lidar or Radar sensors using point cloud registration techniques, such as Normal Distributions Transform (NDT) [3] and Iterative Closest Points (ICP) [2, 22]. For example, Wei et al. [20] proposed a two-stage method for automatic Lidar calibration in road environments. Their approach first perform a coarse calibration using the ground plane, followed by refinement using iterative closest points with normal (ICPN) and octree-based optimization.

Another feasible approach is to leverage entropy to evaluate

Proc. 28th Intn'l Conf. on Information Fusion, Rio de Janeiro, Brazil, July 2025.

the alignment quality of sensor data. Sheehan et al. [18] estimated the environmental distribution using Lidar measurements and optimized geometric alignment by employing Rényi quadratic entropy as a cost function. Meanwhile, Pandey et al. [15] used mutual information between the grayscale values of camera images and the intensity of the Lidar point cloud as the cost function of Lidar-Camera initial calibration.

These entropy-based methods do not rely on any environmental priors, nor require significant computational power, making them well-suited for real-time alignment quality evaluation in autonomous systems. Moreover, based on processing empirical probability distributions of sensor data, they can effectively address the heterogeneity problem of uncertainty of Radar and Lidar point cloud. Therefore, we choose to construct our Radar-Lidar point cloud alignment system based on entropy-based methods.

Additionally, several deep learning based targetless methods have been proposed [4, 9, 17]. However, these methods are highly dependent on specific dataset and may lose effectiveness when sensor types change.

In this paper, we present a targetless Lidar-Radar point cloud alignment system. Our system begins by estimating the distribution of measurements, making the resulting probability density function (PDF) a direct function of the calibration parameters. Then we employ the Rényi Quadratic Entropy (RQE) of the estimated PDF as cost function. Notably, this cost function depends solely on Lidar and Radar measurements, meaning our method does not require any environmental priors. The quality of sensor alignment can be evaluated by monitoring the gradient of the cost function. Finally, we validate the effectiveness and real-time performance of the proposed approach using real-world data. Note that the alignment system is a part of performance evaluation systems of our metrics framework [21].

The remainder of this paper is organized as follows: Section II introduces our alignment system, detailing the theoretical foundations and the algorithmic implementations. Section III presents a series of experiments conducted to validate the effectiveness of our proposed method. Finally, section IV concludes the paper with a summary of findings and point out interesting future work directions.

II. Problem formulation and proposed method

Calibration between heterogeneous sensors and the evaluation of calibration quality are both crucial and challenging tasks for autonomous systems. Lidar and Radar operate based on different perception principles, leading to difference not only in information density but also in measurement uncertainty. In this study, we employ a Gaussian mixture model (GMM) to provide a unified representation for both Radar and Lidar point cloud. The covariance matrix is used to capture and distinguish the difference in perception uncertainty between the two sensor modalities. We then apply RQE to quantify the order and compactness of the resulting PDF. RQE serves both as the cost function for optimizing point-cloud calibration and as a metric for evaluating the quality of sensor alignment.

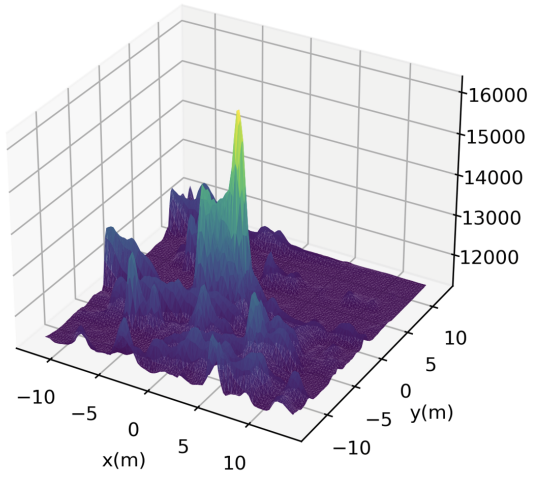

Fig. 1: The negative cost function when $(x_{\mathbf{S}_i}, y_{\mathbf{S}_i})$ changes at specific frame of our dataset.

We assume that the perception environment follows a PDF, denoted as $p(\mathbf{x})$. The corresponding observation point clouds from the Radar-Lidar fusion system are,

$$Z_{\mathbf{S}}^{k} \triangleq \{\mathbf{z}_{\mathbf{S}}(i)\}_{i=1}^{k}, \tag{1}$$

where $\mathbf{S} = \mathbf{R}$ represents the Radar system and $\mathbf{S} = \mathbf{L}$ represents the Lidar system.

By employing a finite mixture model, we assign a Gaussian kernel to each Radar and Lidar point cloud measurement with different covariance values. According to the Parsan window approach [13], the resulting GMM can be expressed as,

$$\begin{aligned} p(\mathbf{x} \mid Z_{\mathbf{S}}^{N_{\mathbf{S}}}) &\approx \frac{1}{N_{\mathbf{S}}} \sum_{i}^{N_{\mathbf{S}}} \mathcal{N}(\mathbf{x}; \mathbf{z}_{\mathbf{S}}(i), P_{\mathbf{S}}) \\ &\triangleq \hat{p}\,(\mathbf{x}), \end{aligned} \tag{2}$$

where $\mathcal{N}(\mathbf{x}; \mu, P)$ represents a Gaussian kernel with mean μ and covariance P.

We utilize the GMM $\hat{p}\,(\mathbf{x})$, as an empirical PDF for the world model $p\,(\mathbf{x})$. This allows us to formulate real-time calibration and alignment as an entropy-based optimization problem. In this task, the objective is to measure the compactness of $p\,(\mathbf{x})$ using RQE [6]

$$H(\mathbf{x}) = -\log \int p^2(\mathbf{x}) d\mathbf{x}, \tag{3}$$

which can be approximated as,

$$\begin{aligned} \hat{H}(\mathbf{x}) &\triangleq -\log \int \hat{p}^2(\mathbf{x}) d\mathbf{x} \\ &= -\log \frac{1}{N_{\mathbf{S}}^2} \\ &\quad \sum_{i=1}^{N_{\mathbf{S}}} \sum_{j=1}^{N_{\mathbf{S}}} \int \mathcal{N}(\mathbf{x}; \mathbf{z}_{\mathbf{S}}(i), P_{\mathbf{S}}) \mathcal{N}(\mathbf{x}; \mathbf{z}_{\mathbf{S}}(j), P_{\mathbf{S}}) d\mathbf{x}. \end{aligned} \tag{4}$$

Then by applying the Gaussian convolution formula

$$\int \mathcal{N}\left(\mathbf{x};\mathbf{x}_i,P_1\right)\mathcal{N}\left(\mathbf{x};\mathbf{x}_j,P_2\right)d\mathbf{x}=\mathcal{N}\left(\mathbf{x}_i;\mathbf{x}_j,P_1+P_2\right), \tag{5}$$

we have

$$\hat{H}(\mathbf{x})=-\log\frac{1}{N_{\mathbf{S}}^2}C(Z_{\mathbf{S}}^{N_{\mathbf{S}}}), \tag{6}$$

where

$$C(Z_{\mathbf{S}}^{N_{\mathbf{S}}})\triangleq\sum_{i=1}^{N_{\mathbf{S_1}}}\sum_{j=1}^{N_{\mathbf{S_2}}}\mathcal{N}(\mathbf{z}_{\mathbf{S_1}}(i);\mathbf{z}_{\mathbf{S_2}}(j),P_{\mathbf{S_1}}+P_{\mathbf{S_2}}). \tag{7}$$

From 6 we note that $\hat{H}(\mathbf{x})$ is simply a monotonic transformation of $C(Z_{\mathbf{S}}^{N_{\mathbf{S}}})$, which is selected as the cost function for the measuring the entropy-based compactness of $p(\mathbf{x})$. And as shown in Fig. 1, although this cost function is not a convex function, it has an obvious minimum for ground translation parameters.

Note that as a cost function for sensor calibration, RQE provides a mathematically tractable and efficient way to measure the compactness of fused Radar-LiDAR point cloud distributions. Unlike Shannon entropy, RQE has a closed-form expression when using Gaussian mixtures, making it suitable for real-time optimization. It requires no environmental priors and works well even with sparse Radar data. By minimizing RQE, the algorithm effectively aligns sensor data, making it ideal for targetless, entropy-based calibration in autonomous systems.

In an autonomous vehicle, there are two primary coordinate systems: the sensor coordinate frame and the vehicle coordinate frame. The coordinates $\mathbf{x}$ and $\mathbf{z}_{\mathbf{S}_i}$ are expressed within the vehicle coordinate frame. Let $\mathbf{z}_{\mathbf{S}_i}^{sc}$ denote the measurements in the sensor coordinate frame of sensor $\mathbf{S}_i$. The inverse sensor model is then given by,

$$\mathbf{z}_{\mathbf{S}_i}=T(\mathbf{\Theta}_{\mathbf{S}_i})\mathbf{z}_{\mathbf{S}_i}^{sc}, \tag{8}$$

where $T(\mathbf{\Theta}_{\mathbf{S}_i})$ denotes the rigid transformation from sensor coordinate frame to the vehicle coordinate frame. This transformation is parameterized by the calibration parameters $\mathbf{\Theta}_{\mathbf{S}_i}\triangleq\{x_{\mathbf{S}_i},y_{\mathbf{S}_i},z_{\mathbf{S}_i},\alpha_{\mathbf{S}_i},\beta_{\mathbf{S}_i},\gamma_{\mathbf{S}_i}\}$ for sensor $\mathbf{S}_i$. By substituting (8) into (7), we obtain the cost function of calibration parameters,

$$\mathbf{E}(\mathbf{\Theta}_{\boldsymbol{S_i}})\triangleq C(\{T(\mathbf{\Theta}_{\mathbf{S}_i})\mathbf{z}_{\mathbf{S}_i}^{sc}\}_{i=1}^{\mathbf{N}}), \tag{9}$$

where $\mathbf{N}$ is the number of sensors.

This cost function serves as a direct metric for calibration quality. It quantifies the compactness of the joint PDF formed by Radar and LiDAR measurements. When the sensors are well calibrated, the fused point clouds align more tightly in space, resulting in a lower entropy value. Conversely, misalignment causes the distribution to spread out, increasing entropy. Therefore, minimizing this cost function corresponds to achieving the best alignment, making it an effective and sensor-agnostic quantitative measure of calibration accuracy.

III. Experiment

A. Dataset

In this section, we validate the algorithm using both the VoD open dataset[14] and our in-house proprietary datasets. The VoD dataset includes a ZF FRGen21 4D Radar and a Velodyne HDL-64 S3 Lidar, providing extrinsic references for all frames. For our dataset, we utilized the following experimental platform[1] as shown in Fig. 2 to capture data.

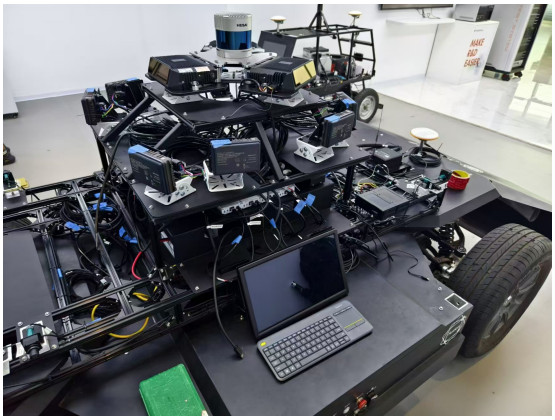

Fig. 2: The experimental platform [19].

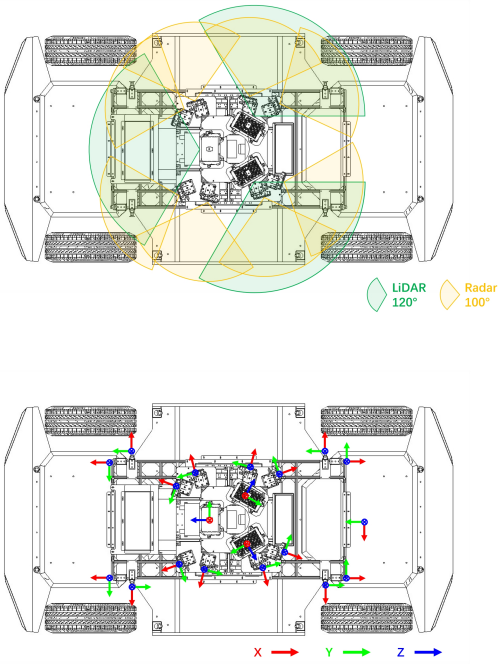

Fig. 3: The FoVs (top) and coordinate frame definition (bottom) of Lidars and Radars.

Our experimental platform consists of an electric chassis equipped with three Innovusion Falcon Kinetic Lidars and

[1]More details about the data center can be found at [19]

eight Continental ARS 548 RDI 4D millimeter wave Radars. The fields of view (FoVs) and coordinate frame definition of the sensors are illustrated in Fig. 3. Both types of sensors operate at a frame rate of 10 fps. The Radar system has a distance measurement accuracy of 0.15m, an azimuth accuracy ranging from 0.1° to 0.5°, and an elevation accuracy of 0.1°. In comparison, the Lidar system has significantly higher accuracy, with a distance measurement precision of 0.02m. In this experiment, we utilized the experimental platform to collect data across 13 different scenarios to validate our algorithm.

B. Experiment Design

Before performing algorithm, we first preprocess the Lidar and Radar point clouds separately. For the Lidar point cloud, we remove ground points that are irrelevant to calibration and system evaluation. For the Radar point cloud, we compensate for Doppler velocity at each point using the velocity measured by the IMU and the initial external reference of the Radar. After compensation, we filter out dynamic points based on the adjusted Doppler velocity.

In this experiment, we assess the registration quality of the Radar-Lidar fusion system by monitoring the gradient of the cost function,

$$\frac{\partial \mathbf{E}(\mathbf{\Theta}|Z_{\mathbf{S}}^{N_{\mathbf{S}}})}{\partial \theta_{\mathbf{S}}} \tag{10}$$

When the gradient exceeds a predefined threshold, the calibration algorithm is triggered to adjust the extrinsic parameters by optimizing the cost function (9).

In the experiment, we use the BFGS quasi-Newton algorithm to optimize (9).The convergence threshold is consistent with the threshold for judging whether the gradient is abnormal, both of which are 10^{-3}. A line search satisfying the strong Wolfe condition is used at each iteration to ensure that the Hessian remains approximately positive definite. To prevent numerical oscillation or excessive computation, we also set the maximum number of iterations to $N_{\max} = 100$ to ensure proper algorithm termination.

During the optimization process, we set the sensor covariances as $P_{\mathbf{S}} = \sigma_{\mathbf{S}}^2 I$, assuming that individual sensors are isotropic. When computing the cost function, we consider only point pairs within a distance of $k\sigma_{\mathbf{S}}$. This significantly enhances the computational efficiency of the algorithm [12]. In the experiment, we utilize a KD-tree to efficiently search for eligible point pairs.

For the VoD dataset, we set the Lidar uncertainty to $\sigma_{\mathbf{L}} = 0.1m$ and the Radar uncertainty to $\sigma_{\mathbf{R}} = 0.5m$. Since the dataset utilizes a mechanical Lidar with a 360 degree FoV, we treat the Lidar point cloud as the reference frame and calibrate the Radar accordingly. For our own dataset, we performed calibration across 13 different scenarios, setting the Lidar uncertainty to $\sigma_{\mathbf{L}} = 0.05m$ and the Radar uncertainty to $\sigma_{\mathbf{R}} = 0.2m$. When an abnormal gradient in the cost function is detected, we fix all sensors except the one exhibiting the anomaly, treating the stable sensors as the reference frame and calibrating the abnormal sensor accordingly. To thoroughly validate the robustness of the algorithm, we initialize the extrinsic parameters of all sensors with values that are expected to produce anomalous gradients.

C. Calibration Results

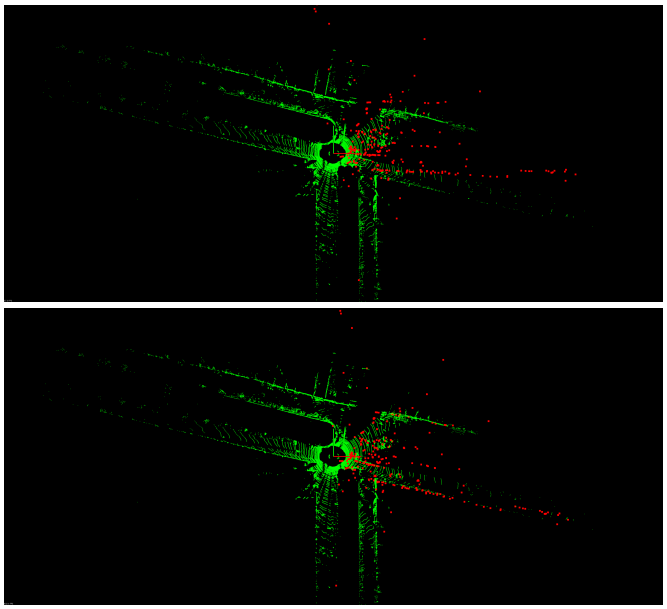

Fig. 4: The initial state (top) and calibration results (bottom) of VoD dataset.

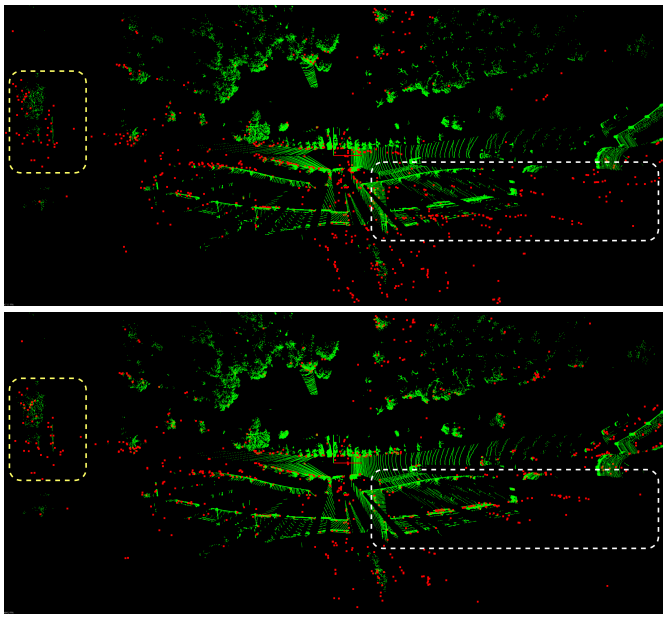

Fig. 5: The initial state (top) and calibration results (bottom) of our in-house dataset. The results show that mainly the extrinsic parameters of the Radar point cloud within the dashed box are corrected.

Figs. 4 and 5 show the calibration results for a specific frame, where green dots represent Lidar measurement points

and red dots represent Radar measurement points. To highlight the improvement, the system was initialized with a deliberately poor extrinsic configuration. In Fig. 4, the calibration results are clearly visible. In the highlighted region (white box) of Fig. 5, the Lidar and Radar point clouds corresponding to a wall are initially misaligned due to incorrect parameters. After the calibration algorithm converges, the point clouds closely overlap, demonstrating the effectiveness of the proposed method.

TABLE I: The Calibration Results with $\sigma_{\mathbf{L}} = 0.05$ and $\sigma_{\mathbf{R}} = 0.2$

	Lidar			Radar		
	seed[a]	mean	std dev	seed	mean	std dev
x(m)	1.2	0.875	0.208	1.3	1.015	0.181
y(m)	0.0	-0.171	0.130	0.3	0.023	0.214
z(m)	1.0	0.560	0.231	0.0	-0.364	0.498
roll(°)	120	124.685	0.443	0	6.812	1.980
pitch(°)	0.0	0.392	0.116	0	0.304	1.336
yaw(°)	120	127.761	0.230	20	18.769	0.288

[a]For simplicity, the mean value in the table belongs to the front Lidar and the left front Radar, respectively, while the standard deviation is the statistical result of all sensors of the same type.

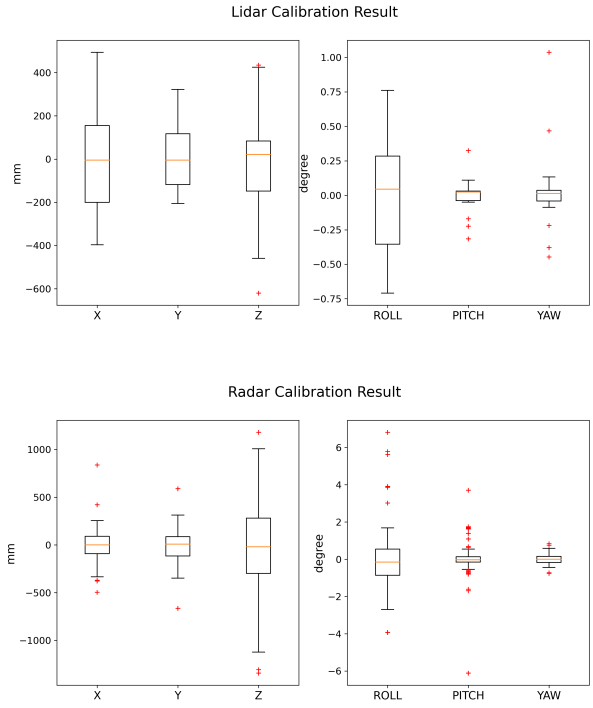

Fig. 6: The Boxplot of Lidar and Radar Calibration Results. For simplicity, we merged the results of the same type of sensors into a single boxplot after subtracting their own mean results.

Table I and Fig. 6 present the distribution of calibration results across 13 scenarios in our datasets. For simplicity, we merged the results of the same type of sensors into a single boxplot after subtracting their mean results. The boxplots show very few outliers, indicating that our algorithm demonstrates a certain level of robustness. However, the algorithm's performance on translation parameters is obviously inferior to its performance on rotation parameters. Additionally, its overall performance is weaker compared to the 2D-3D Lidar system. This discrepancy primarily arises from the sparsity of Radar point clouds, which makes Radar points more likely to be attracted to denser regions of the Lidar point cloud during calibration, rather than aligning with their true physical correspondences in the real world. This effect is particularly pronounced in the estimation of translation parameters.

IV. Conclusions

In this paper, we proposed a targetless real-time Radar-Lidar point cloud alignment system and validated its effectiveness using real-world data. The method does not rely on any environmental priors and it can be deployed in a wide range of environments, making it particularly suitable for sanity/healthy checks and calibration corrections in autonomous systems.

However, the algorithm's performance on translation parameters is notably weaker than on rotation parameters. In real-world scenarios, where factors such as fixture aging may affect sensor alignment, translation shifts typically occur on the centimeter scale. We currently use this algorithm primarily for correcting rotational extrinsic parameters in Lidar-Radar fusion systems and will refine the approach to a more general case.

A key limitation of the algorithm is the sparsity of the Radar point cloud, which affects calibration performance. In addition, the algorithm currently operates on a single frame basis when correcting extrinsic parameters. Incorporating temporal information by leveraging multiple frames over a time series, especially when abnormal gradients are detected, could help compensate for Radar sparsity. Addressing this limitation will be an important future direction of our research.

References

[1] P. An, T. Ma, K. Yu, B. Fang, J. Zhang, W. Fu, and J. Ma, "Geometric calibration for LiDAR-camera system fusing 3D-2D and 3D-3D point correspondences", *Optics express*, Vol. 28, No. 2, pp. 2122–2141, 2020.

[2] P. J. Besl and N. D. McKay, "Method for registration of 3-D shapes", *Sensor Fusion IV: Control Paradigms and Data Structures*. Vol. 1611, pp. 586 –606, 1992.

[3] P. Biber and W. Strasser, "The normal distributions transform: a new approach to laser scan matching", *Proceedings 2003 IEEE/RSJ International Conference on Intelligent Robots and Systems (IROS 2003)*. Vol. 3, pp. 2743–2748, 2003.

[4] O. Bogdan, V. Eckstein, F. Rameau, and J.-C. Bazin, "DeepCalib: a deep learning approach for automatic intrinsic calibration of wide field-of-view cameras", *Proceedings of the 15th ACM SIGGRAPH European Conference on Visual Media Production*, 2018.

[5] D.-G. Choi, Y. Bok, J.-S. Kim, and I. S. Kweon, "Extrinsic calibration of 2-d lidars using two orthogonal planes", *IEEE Transactions on Robotics*, Vol. 32, No. 1, pp. 83–98, 2015.

[6] G. E. Crooks, "On measures of entropy and information", *Tech. Note*, Vol. 9, No. 4, 2017.

[7] C. Gao and J. R. Spletzer, "On-line calibration of multiple lidars on a mobile vehicle platform", *2010 IEEE International Conference on Robotics and Automation*, pp. 279–284, 2010.

[8] A. Geiger, F. Moosmann, Ö. Car, and B. Schuster, "Automatic camera and range sensor calibration using a single shot", *2012 IEEE international conference on robotics and automation*, pp. 3936–3943, 2012.

[9] G. Iyer, R. K. Ram, J. K. Murthy, and K. M. Krishna, "CalibNet: Geometrically Supervised Extrinsic Calibration using 3D Spatial Transformer Networks", *2018 IEEE/RSJ International Conference on Intelligent Robots and Systems (IROS)*, pp. 1110–1117, 2018.

[10] T. Kim and T. Park, "Calibration method between dual 3D lidar sensors for autonomous vehicles", *2017 56th Annual Conference of the Society of Instrument and Control Engineers of Japan (SICE)*, pp. 1075–1081, 2017.

[11] T. Ma, Z. Liu, G. Yan, and Y. Li, "Crlf: Automatic calibration and refinement based on line feature for lidar and camera in road scenes", *arXiv preprint arXiv:2103.04558*, 2021.

[12] W. Maddern, A. Harrison, and P. Newman, "Lost in translation (and rotation): Rapid extrinsic calibration for 2d and 3d lidars", *2012 IEEE International Conference on Robotics and Automation*, pp. 3096–3102, 2012.

[13] G. J. McLachlan and D. Peel. *Finite mixture models*. Vol. 299. 2000.

[14] A. Palffy, E. Pool, S. Baratam, J. F. Kooij, and D. M. Gavrila, "Multi-class road user detection with 3+1D radar in the View-of-Delft dataset", *IEEE Robotics and Automation Letters*, Vol. 7, No. 2, pp. 4961–4968, 2022.

[15] G. Pandey, J. McBride, S. Savarese, and R. Eustice, "Automatic targetless extrinsic calibration of a 3d lidar and camera by maximizing mutual information", *Proceedings of the AAAI conference on artificial intelligence*. Vol. 26, No. 1, pp. 2053–2059, 2012.

[16] J. Peršić, I. Marković, and I. Petrović, "Extrinsic 6DoF calibration of 3D LiDAR and radar", *2017 European Conference on Mobile Robots (ECMR)*, pp. 1–6, 2017.

[17] N. Schneider, F. Piewak, C. Stiller, and U. Franke, "RegNet: Multimodal sensor registration using deep neural networks", *2017 IEEE Intelligent Vehicles Symposium (IV)*, pp. 1803–1810, 2017.

[18] M. Sheehan, A. Harrison, and P. Newman, "Automatic self-calibration of a full field-of-view 3D n-laser scanner", *Experimental Robotics: The 12th International Symposium on Experimental Robotics*, pp. 165–178, 2014.

[19] SJTU SSF Lab. *SJTU Smart Data Center*. Accessed on June 1st, 2025. URL: http://cadar.ai.

[20] P. Wei, G. Yan, Y. Li, K. Fang, X. Cai, J. Yang, and W. Liu, "Croon: Automatic multi-lidar calibration and refinement method in road scene", *2022 IEEE/RSJ International Conference on Intelligent Robots and Systems (IROS)*, pp. 12857–12863, 2022.

[21] X. Yuxuan, F. García-Fernández, J. Karlsson, K.-C. Chang, T. Yuan, and L. Svensson, "Probabilistic GOSPA: A metric for performance evaluation of multi-object filters with uncertainties", *IEEE Transactions on Aerospace and Electronic Systems*, pp. accepted with revisions, 2025.

[22] Z. Zhang. *Iterative point matching for registration of free-form curves*. Research Report RR-1658. INRIA, 1992, pp. 42.

[23] L. Zhou, Z. Li, and M. Kaess, "Automatic extrinsic calibration of a camera and a 3d lidar using line and plane correspondences", *2018 IEEE/RSJ International Conference on Intelligent Robots and Systems (IROS)*, pp. 5562–5569, 2018.

[24] Y. Zhu, C. Li, and Y. Zhang, "Online Camera-LiDAR Calibration with Sensor Semantic Information", *2020 IEEE International Conference on Robotics and Automation (ICRA)*, pp. 4970–4976, 2020.